Effect of gedunin on glioblastoma proliferation and invasiveness: *In vitro* and *in vivo* approaches

Thadeu Estevam Moreira Maramaldo Costa[a,b], Tatiana Almeida Pádua[b], Jonathas Xavier Pereira[c], Vinicius Gonçalves Rodrigues[c], Leonardo Noboru Seito[b], Erika Marques da Cunha[b], Claudio C. Filgueiras[d], Yael Abreu-Villaça[d], Alex C. Manhães[d], Clarissa Menezes Maya-Monteiro[e], Maria das Graças Henriques[b,f], Thomas Eichenberg Krahe[d,g], Carmen Penido[a,b,*]

[a] Centro de Desenvolvimento Tecnológico em Saúde, Instituto Nacional de Ciência e Tecnologia de Inovação em Doenças Negligenciadas (INCT-IDN), Fundação Oswaldo Cruz, Rio de Janeiro, Brazil.

[b] Laboratório de Farmacologia Aplicada, Instituto de Tecnologia em Fármacos (Farmanguinhos), Fundação Oswaldo Cruz, Rio de Janeiro, Brazil.

[c] Instituto de Patologia Tropical e Saúde Pública (IPTSP), Universidade Federal de Goiás (UFG), Goiás, Goiânia, Brasil.

[d] Laboratório de Neurofisiologia, Departamento de Ciências Fisiológicas, Instituto de Biologia Roberto Alcantara Gomes, Universidade do Estado do Rio de Janeiro (UERJ), Rio de Janeiro, Brazil.

[e] Laboratório de Imunofarmacologia, Instituto Oswaldo Cruz (IOC), Fundação Oswaldo Cruz, Rio de Janeiro, Brazil.

[f] Laboratório de Farmacologia Celular e Molecular, Departamento de Biologia Celular; Instituto de Biologia Roberto Alcântara Gomes, Universidade do Estado do Rio de Janeiro (UERJ), Rio de Janeiro, Brazil.

[g] Departamento de Psicologia, Pontifícia Universidade Católica do Rio de Janeiro (PUC-Rio), Rio de Janeiro, Brazil.

[*]**Address correspondence to**: Dr. Carmen Penido, Laboratório de Farmacologia Aplicada, Departamento de Farmacologia Aplicada, Farmanguinhos, Fundação Oswaldo Cruz, Rua Sizenando Nabuco 100, Manguinhos, Rio de Janeiro, RJ, CEP 21041-250, Brazil, e-mail: cpenido@gmail.com; carmen.penido@fiocruz.br.

Graphical Abstract

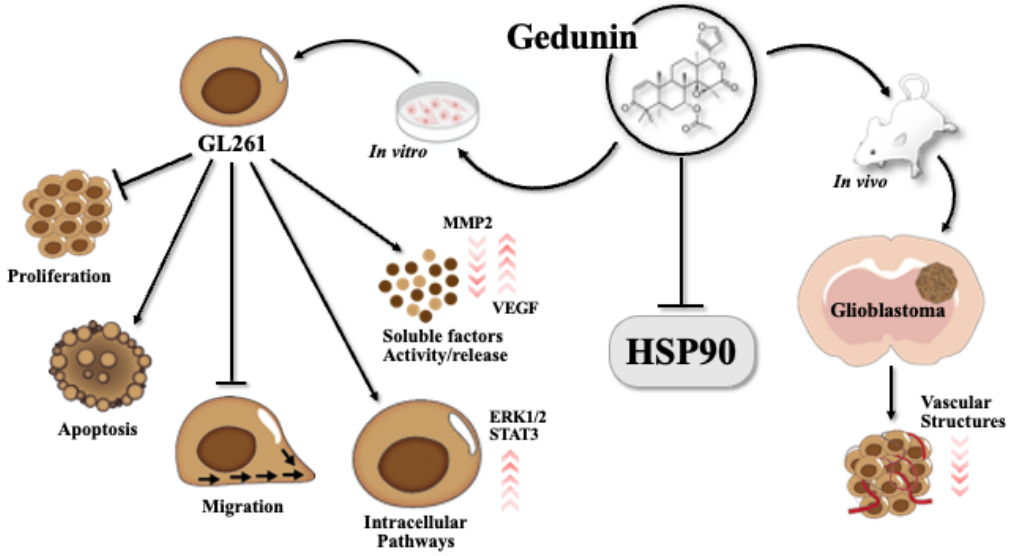

Highlights

- Gedunin reduces GL261 cell proliferation, migration and invasion *in vitro*.
- Gedunin induces GL261 cell apoptosis and ERK activation *in vitro.*
- Gedunin reduces the presence of tumoral vascular structures *in vivo.*

Abstract

Glioblastoma is the most invasive and malignant brain tumor, for which no effective treatment is currently available. Heat shock protein 90 (HSP90) is a potential target for the treatment of different types of cancer. Herein, we investigated the effect of gedunin, an HSP90 inhibitor, in murine GL261 glioblastoma *in vitro* and *in vivo* models. Gedunin treatment decreased GL261 cell proliferation and triggered apoptosis in a concentration-dependent manner. Gedunin also reduced GL261 cell migration and metalloproteinase-2 activity, suggesting that it impairs glioblastoma cell invasion. Despite the reduction of total protein content in gedunin-treated cells, the phosphorylation of STAT3 and ERK1/2 pathways was enhanced within 24 h. *In situ* treatment with gedunin did not significantly

reduce tumor volume but reduced the presence of vascular structures in xenograft glioblastoma in C57BL/6 mice, a clinical feature associated with morbidity and mortality. Our results demonstrate that gedunin is a promising compound for the treatment of glioblastoma.

Keywords: Brain tumor, GL261, limonoids, natural products.

1. Introduction

Glioblastoma is a highly invasive and malignant tumor defined by the World Health Organization as grade IV, based on histological, immunohistochemical, and molecular features [1]. Patients bearing glioblastoma have a poor prognosis, with estimated median survival rates of eight months and a maximum five-year survival rate of only 5% [2,3].

The current standard protocol for glioblastoma treatment relies on total tumor excision followed by radiotherapy with concurrent and adjuvant chemotherapy with temozolomide [4]. The most common adverse events related to temozolomide treatment are myelosuppression and hepatotoxicity [5–7]. Another limiting factor of glioblastoma treatment is that most orally and intravenously administered alkylating agents induce resistance and have poor blood-brain barrier permeability [8,9]. An alternative strategy is the usage of intracranial wafer implants containing the alkylating agent carmustine after tumor removal surgery, which, in combination with radiochemotherapy, has been shown to significantly improve patient survival [10,11]. However, carmustine wafers induce severe side effects, such as cerebral edema and hematological toxicity [5,12,13]. Glioblastoma is still considered incurable [14]; however, treatments targeting multiple signaling pathways are a promising strategy [15].

Modulation of the chaperone heat shock protein 90 (HSP90) is considered a potential antitumor therapy [16]. HSP90 activity is implicated on several hallmarks of cancer, such as proliferation, invasion, metastasis, angiogenesis, and resistance to apoptosis [17]. Increased expression of HSP90 correlates with tumor malignancy and poor prognosis in different types of cancer, including breast, colon, and melanoma [18–21]. Indeed, HSP90 chaperones several proteins involved in oncogenic processes, including the human epidermal growth factor receptor 2 (HER2/neu; ErbB2), tyrosine-protein kinase Src (Src), protein kinase B (AKT/PKB), breakpoint cluster region/Abelson murine leukemia virus (BCR/ABL) and tumor protein 53 (p53) [22–24]. In line with this, encouraging pre-clinical data have been obtained with HSP90 inhibitors in different types of tumor cells and animal models, including lymphoma, melanoma, breast, and lung cancer [25–29]. Currently, in the NIH´s Clinical Trials database ClinicalTrials.gov, there are more than a hundred registered trials (11 currently active) evaluating HSP90 inhibitors (alone or in combination with other drugs) for the treatment of different types of cancer [30]. Worthy

102 of note, off-target toxicity, including ocular toxicity and hepatotoxicity, is a limiting
103 factor for the use of these substances [31,32].

104 Over the past two decades, our group and others have been studying the antitumoral and
105 anti-inflammatory effects of gedunin, a limonoid produced by vegetal species from the
106 Meliaceae family [33] or by semi-synthetic routes [34]. Gedunin negatively modulates
107 HSP90 activity by binding to the HSP90 co-chaperones p23 and cdc37 and, thus,
108 impairing the formation of the active HSP90 complex [35,36]. This limonoid has potent
109 antitumoral effects demonstrated against an array of tumor types *in vivo* and *in vitro*
110 [35,37–40]. However, gedunin anti-tumoral effects have not been evaluated in
111 glioblastoma.

112 Considering the urgent need for an effective therapy against glioblastoma and the high
113 antitumor activity of the HSP90 inhibitor gedunin, here we investigate the antitumoral
114 effect of this compound using the murine GL261 model both *in vitro* and *in vivo*.

115

116 **2. Materials and Methods**

117 ***2.1 Reagents and antibodies***

118 Gedunin (Gaia Chemicals, USA) and the specific HSP90 inhibitor 17-AAG (17-N-
119 allylamino-17-demethoxygeldanamycin, Tanespimycin, Sigma-Aldrich, USA) were
120 dissolved in DMSO (dimethyl sulfoxide, Sigma-Aldrich) and frozen at -86 °C until use.
121 MTT (3-(4,5-dimethylthiazol-2-yl)-2,5-diphenyl tetrazolium bromide), Dulbecco´s
122 modified Eagle´s medium (DMEM), phosphate buffer saline (PBS) tablet and trypsin-
123 EDTA (ethylenediamine tetraacetic acid) solution were purchased from Sigma Aldrich.
124 Fetal bovine serum (FBS) was purchased from Cultilab (Brazil). Propidium iodide (PI)
125 solution was obtained from Biolegend (USA). Vybrant™ CFDA-SE (carboxyfluorescein
126 diacetate succinimidyl ester) Cell Tracer Kit and gentamicin were obtained from Thermo
127 Fischer Scientific (USA). Annexin V-FITC (fluorescein isothiocyanate) conjugated was
128 purchased from BD Pharmingen (USA). IgG anti-mouse STAT3 (signal transducer and
129 activator of transcription 3, rabbit, C-20), anti-mouse-IgG-HRP (horseradish peroxidase),
130 and anti-rabbit-IgG-HRP secondary antibodies were purchased from Santa Cruz
131 Biotechnologies (USA). Antibodies against mouse p44/42 MAPK (mitogen-activated
132 protein kinase, Thr202/Tyr204, D13.14.4E), ERK1/2 (extracellular signal-regulated
133 kinase 1/2, rabbit), AKT (protein kinase B, PKB, rabbit, pan, 40D4), phospho-AKT
134 [rabbit, Ser473, (D9E)XP] and GAPDH (glyceraldehyde-3-phosphate
135 dehydrogenasemouse, D4C6R) were purchased from Cell Signaling (USA). Antibodies
136 against human PCNA (proliferating cell nuclear antigen, rabbit) were purchased from
137 Sino Biological (China). DNase I recombinant RNase free was purchased from Roche
138 Life Sciences (Germany).

139

140 ***2.2 GL261 cell culture and treatment***

141 Murine glioblastoma cell line (GL261, Cell Bank from Federal University of Rio de
142 Janeiro - UFRJ, Brazil) was cultured in DMEM (Sigma Aldrich) supplemented with 10
143 % FBS (Cultilab) and 50 µg/mL gentamicin (Thermo Fisher Scientific) in humidified
144 atmosphere (5 % CO_2 at 37 °C) until confluence. Cells were digested with 0.25 % trypsin
145 at the 5th passage and washed with 1x PBS. Cell viability was determined by trypan blue
146 (Sigma Aldrich) staining, under a light microscope, before further assays. GL261 cells
147 were incubated with 6.25-100 µM of gedunin for 24-72 h at 37 °C, 5 % CO_2.

148

149 ***2.3 Animals***

150 Adult male C57BL/6 mice (20-25 g) provided by Oswaldo Cruz Foundation (Fiocruz)
151 breeding unit (Institute for Biomodels Science and Technology, Rio de Janeiro, Brazil)
152 were kept in standard autoclavable polypropylene boxes, with free access to food and
153 fresh water in environmentally controlled room temperature (ranging from 22 to 24 °C)
154 on a light/dark cycle at Farmanguinhos (Fiocruz, Rio de Janeiro, Brazil) and at the
155 Laboratory of Neurophysiology (State University of Rio de Janeiro, Rio de Janeiro,
156 Brazil) experimental animal facilities. Animal procedures were performed in accordance
157 with the ethical guidelines of the Brazilian National Council for the Control of Animal
158 Experimentation (CONCEA) and reported following the ARRIVE guidelines [41].
159 Experimental procedures were approved by the Ethics Commission on Animal Use of
160 Oswaldo Cruz Foundation (license #LW-35/16) and the Ethics Commission on Animal
161 Use of the State University of Rio de Janeiro (license #025/2017).

162

163 ***2.4 Primary mixed glial cell culture***

164 Under sterile conditions, mouse brain cortex tissue was rapidly dissected from euthanized
165 (150 mg/kg sodium thiopental, i.p.) young adult (4-week-old) C57BL/6 male mice and
166 transferred to ice-cold DMEM/F12 media (Sigma Aldrich) in 6 well plates. After removal
167 of the meninges, brain tissue was cut into small pieces, and washed three times with 1x
168 sterile PBS (Sigma Aldrich). Trypsin-DNAse solution (0.25 %-250 µg/mL) was added to
169 the wells and the plate was incubated for 1 h in an orbital shaker (Excella E24, New
170 Brunswick Scientific, USA) at 37 °C and 150 rpm. Tissue samples were vigorously
171 triturated and dissociated with a 1 mL pipette tip. Cells were washed with FBS-DNAse
172 solution (10 %-250 µg/mL), added to a 20 % percoll gradient media, and centrifuged at
173 800 × *g* for 30 min at 25 °C. Recovered cells were washed (400 × *g*, 10 min at 4 °C),
174 distributed in T-25 bottle flasks, and incubated at 37 °C, 5 % CO_2. DMEM/F12 media
175 was changed every 3-4 days until use. Data were collected from two independent
176 experiments (n=5 mice per group; license #LW-35/16).

177

178 ***2.5 Proliferation assay***

179 GL261 cells (4 × 10^7/mL) were incubated with 5 μM CFSE solution (Invitrogen
180 Molecular Probes, USA) diluted in PBS for 15 min at 37 °C, 5 % CO_2. Cells were washed
181 with 10 % PBS/FBS solution, seeded in 24 well plates (2 × 10^5 cells per well), incubated
182 overnight, and treated with gedunin (6.25-100 μM) for 72 h. Cell proliferation was
183 evaluated by analyzing CFSE fluorescence intensity (FL1) upon cell divisions, by flow
184 cytometry (FACScalibur, Becton Dickinson, USA). Results were analyzed using FlowJo
185 X Software (Tree Star, Becton Dickinson).
186
187 ***2.6 MTT assay***
188 GL261 or primary mixed glial cells were seeded in a 96 flat bottom well plate (2 × 10^4
189 cells/well) and cultured in DMEM for 24 h (CO_2 5 % at 37 °C) for adhesion. Adherent
190 cells were cultured with different concentrations of gedunin (6.25-100 μM), 17-AAG (1
191 μM), or temozolomide (100 μM) for 20 or 68 h, when MTT solution (5 mg/mL; 22.5
192 μL/well) was added to the culture and incubated for 4 h. The analyzes were performed at
193 24 and 72 h time points. Plates were centrifuged for 3 min (720 × *g* at 4 °C), the
194 supernatant was discharged and DMSO (150 μL/well) was added for formazan crystals
195 solubilization. The absorbance was read in a microplate reader (SpectraMax M5,
196 Molecular Devices, USA) at 540 nm.
197
198 ***2.7 Determination of apoptosis***
199 Apoptosis was evaluated using annexin V-FITC and propidium iodide (PI) staining.
200 GL261 cells were seeded in 24 well cell culture plates (2 ×10^5 cells/well) and left to
201 adhere overnight. GL261 cells were then incubated with gedunin (6.25 - 100 μM) for 24
202 or 72 h, followed by trypsinization, resuspension in annexin V Binding Buffer (HEPES
203 10 mM pH 7.4, NaCl 140 mM, $CaCl_2$ 2.5 mM) and labeling with annexin V-FITC and PI
204 for 15 min at room temperature. Cells incubated with medium were used as the negative
205 control, whereas 17-AAG-incubated cells were used as the positive control. Staining was
206 analyzed by cytometry using FACScalibur (Becton Dickinson) and FlowJo Software
207 (Tree Star, Becton Dickinson). At least 10^4 cells were acquired per sample. Data are
208 presented in dot plots in a log scale of increasing FL-1 (annexin V-FITC) and FL-3 (PI)
209 intensity.
210

211 ***2.8 Scratch assay***

212 GL261 cell monolayers, seeded into 6 well plates, were scratched at the center of the well,
213 and then the migration path was assessed at the leading edge of the scratch by phase-
214 contrast optical microscopy (100 ×, Olympus IX70, Japan) at indicated time points.
215 Analyses were performed by Image J software (National Institute of Health, USA). The
216 rate of migration was determined by quantifying the total distance that cells moved from
217 the edge of the scratch toward the center of the scratch, as previously described [42].
218

219 ***2.9 Chemotaxis assay***

220 GL261 cell migration was assayed in a 48-well micro-chemotaxis Boyden chamber
221 (Neuro Probe Inc., USA). The bottom wells of the chamber were filled with DMEM 10
222 % FBS (29 μL) or serum-free DMEM media as the negative control. Polycarbonate
223 membrane filters with 8 μm pore size (Neuro Probe) were placed between the lower and
224 upper chambers. GL261 cells were pre-treated with different concentrations of gedunin
225 (6.25-25 μM) for 1 h in serum-free DMEM and then loaded into the upper wells of
226 Boyden chamber (2×10^4 cells/50 μL/well). The chamber was incubated in a humidified
227 atmosphere with 5 % CO_2 at 37 °C for 24 h. The membranes were removed and stained
228 using a Diff-quick (Laborclin, Brazil). The bottom side of membranes was visualized by
229 light microscopy for counting GL261 migrating cells (1000 ×, Olympus IX70). GL261
230 chemotaxis was calculated and expressed as the mean number of migrated cells in ten
231 random high-power fields (HPFs) per well (in quadruplicate).
232

233 ***2.10 Zymography***

234 GL261 cells were plated (1×10^6/well) in a 6-well plate in DMEM. After 24 h,
235 supernatant was removed, and cells were washed 3 times with pure DMEM to eliminate
236 any FBS trace. Then, cells received gedunin (6.25-50 μM) or 17-AAG (1 μM) treatment
237 in serum-free DMEM. After 48 h, the supernatant was collected and stored at -70 °C until
238 lyophilization. Samples were dehydrated in a Gamma 2-16 LSCplus (Christ, Germany)
239 ice condenser and, resuspended with 200 μL of zymography extraction buffer (Tris-HCl
240 50 mM pH 7.5, NaCl 0.2 M, Triton X-100 0.1 %, $CaCl_2$ 10 mM, protease inhibitor
241 cocktail). Lowry method was used for protein quantitation. Enzymatic activity of matrix

242 metalloproteinase (MMP)-2 was determined on a 10 % SDS-PAGE containing 0.1 %
243 gelatin from porcine skin (Sigma Aldrich).
244
245 ***2.11 Enzyme-linked immunosorbent assay***
246 Levels of vascular endothelial growth factor (VEGF) were evaluated by sandwich
247 enzyme-linked immunosorbent assay (ELISA) in GL261 cell supernatants using
248 matched antibody pairs from R&D Systems (USA), according to the manufacturer's
249 instructions. Absorbance was determined by Spectramax M5 microplate reader
250 (Molecular Devices) at 490 nm.
251
252 ***2.12 Western blot***
253 GL261 cells (1×10^5 cells) treated with gedunin (6.25-100 μM) or 17-AAG (1 μM) for
254 24 h were lysed in a buffer containing protease inhibitors. Protein extract (20 μg) was
255 resolved by SDS-PAGE, proteins were transferred to polyvinylidene difluoride (PVDF)
256 membranes (GE Healthcare, USA), and then probed with primary antibodies. Antibodies
257 were diluted in Tris-buffered saline containing 0.5 % Tween 20 and 5 % non-fat milk or
258 bovine serum albumin (BSA, Sigma -Aldrich, USA), and incubated overnight at 4 °C.
259 The membranes were incubated with horseradish peroxidase (HRP)-conjugated
260 secondary IgG (Santa Cruz Biotechnology) for 1 h at room temperature. The blots were
261 developed in a Hyperfilm with the use of a chemiluminescent substrate (ECL; Amersham
262 Biosciences, USA). The band intensity was quantified using ImageJ (NIH, USA), and
263 expressed in arbitrary units (a.u.). The raw intensity values of total proteins were
264 normalized using the values of the control protein (PCNA) and of the control group
265 (untreated cells) to allow comparison between different experiments. The phospho-
266 protein values were normalized by the specific total-protein content. Western blot
267 membranes were stripped using harsh stripping buffer (SDS 10% Tris HCl, pH 6.8, 0.5
268 M; 0.8 % ß-mercaptoethanol), at 50 °C for up to 45 min under agitation in an orbital
269 shaker (Excella E24, New Brunswick Scientific, USA). Stripping was performed between
270 the phospho and total proteins, and between AKT and ERK antibody incubations.
271
272 ***2.13 Orthotopic glioblastoma model and osmotic mini-pump implantation***

273 Glioblastoma was induced in adult male C57BL/6 by stereotaxic injections of GL261
274 cells at the Laboratory of Neurophysiology experimental animal facility (UERJ, Rio de
275 Janeiro, Brazil). Mice were intraperitoneally anesthetized with 100 mg/kg ketamine
276 (Syntec, Brazil) and 10 mg/kg xylazine (Sedalex™ Venco, Brazil). Under sterile
277 conditions, a midline incision was made in the scalp, the skull was exposed to identify
278 bregma and lambda, and a small burr hole was drilled over the right hemisphere. GL261
279 cells (5×10^4/μL; final volume of 2 μL) were stereotaxically injected into the caudate
280 putamen with a 10 μL Hamilton syringe at the rate of 0.5 μL/min. The needle was slowly
281 removed 4 min after the injection was finished. The following coordinates (in mm) were
282 used for stereotaxic injections (anterior-posterior; medial-lateral; dorsal-ventral): 0.1
283 AP; 2.32 ML; 2.35 DV. Coordinates were based on the Cha et al., 2003 [43] descriptions
284 and confirmed on Paxinos and Franklin mouse brain atlas [44]. Fourteen days after
285 GL261 injections, animals were implanted with Alzet osmotic minipumps (model 2004,
286 0.25 μL/h; Durect Corporation, USA) filled with gedunin (250 μM, n=8) or DMSO (2.5
287 %, n=8). Cannulas (1-2 mm long) were placed into the site of the tumor following similar
288 surgical procedures described above. Treatment lasted between 14 and 17 days. Mice
289 were monitored every day for clinical signs of pain and distress, such as ruffled fur,
290 hunched back, trembling, convulsions, paralysis, and permanent recumbency [45]. If
291 signs of pain and distress were observed, the animal was excluded from the study and
292 euthanized. Data were collected from two independent experiments (n=8 randomized
293 mice per group). Mice were euthanized 28 days after GL261 injection with sodium
294 thiopental (150 mg/kg, i.p.).
295
296 ***2.14 Mouse Brain Computed Tomography Images***
297 After 14-day treatment, anesthetized mice (100 mg/kg ketamine/10 mg/kg xylazine, i.p.)
298 were intravenously (i.v.) injected with 300 mg/mL of Omnipaque iohexol contrast (GE
299 Healthcare). Brains were scanned 3-6 min after contrast administration in a GE Highspeed
300 CT/E image system (Pedro Ernesto University Hospital, UERJ, Rio de Janeiro, Brazil),
301 according to the following protocol: 120 kV tube voltage, 55 mA, 1 mm slice thickness.
302 Images were reconstructed in a 256 x 256-pixel matrix using InVesalius 3.1.1 software
303 (developed by Centro de Tecnologia da Informação Renato Archer, CNPq, and Ministry

304 of Health, Brazil). Tumor volumetry was determined by selecting contrast-enhanced
305 regions of interest in coronal sections.
306
307 ***2.15 Histology of Brain Tissue***
308 Euthanized mice (150 mg/kg sodium thiopental, i.p.) were perfused with 4%
309 formaldehyde. Mouse brains were collected and transferred into a 4 % formaldehyde
310 solution for 2 days for tissue fixation. Brains were then sectioned and embedded in
311 paraffin. Coronal sections of brain tissue (5 μm) were made using a Shandon Finesse 325
312 microtome (Thermo Fisher Scientific). Brain slices were stained with hematoxylin
313 (Merck, USA) and eosin (Sigma Aldrich, USA). Lesion size, liquefactive necrosis area,
314 vascular structures, intratumoral hemorrhage, and mitosis were blindly analyzed in the
315 central slice tumor area. Lesion size area was defined by the percentage of tumor area in
316 relation to the size of the brain area in the slice. The liquefactive necrosis area was
317 determined by the percentage of necrosis area in relation to the lesion size. Vascular
318 structures that had their full composition were counted in intratumoral and peritumoral
319 regions. Intratumoral hemorrhage was described in a semi-quantitative form regarding
320 the intensity at the slice, with the following definitions: discrete (+), moderate (++), and
321 intense (+++). Mitosis was characterized by estimating the average amount of cells per
322 analyzed field, and thus: >50% (+), 50-75% (++), and >75% (+++). Multipoint brain slice
323 images were composed in NIS-Elements AR (Nikon Corporation). Each brain slice was
324 analyzed by an observer blind to the experimental groups.
325
326 ***2.16 Statistical Analysis***
327 All analyzes were performed using GraphPad Prism 5 (GraphPad Software, USA).
328 Western blot analyzes were performed using the non-parametric Kruskal-Wallis test
329 followed by Dunn's multiple comparisons. Histologic analyzes were performed by one-
330 way analysis of variance (ANOVA) and Tukey's post-test for multiple comparisons. All
331 other comparisons were carried out using one-way ANOVA followed by Student-
332 Newman-Keuls test. Data are shown as the mean $\pm$ SEM (unless otherwise mentioned).
333 Significance was assumed either at the level of $p \leq 0.05$, $p \leq 0.01$, or $p \leq 0.001$, as
334 specified.
335

336 **3. Results**

337 ***3.1 Gedunin impairs GL261 cell growth and viability in vitro***

338 To verify the effect of gedunin on GL261 cell growth, a 72 h CFSE proliferation assay
339 was performed, in which staining decreases as cells proliferate. Incubation of CFDA-SE-
340 stained GL261 cells with gedunin decreased cell proliferation in a concentration-
341 dependent manner (**Fig. 1A**). Gedunin (25-100 μM) significantly inhibited GL261 cell
342 growth, similar to what was observed with the selective HSP90 inhibitor 17-AAG
343 (reference control). **Figure 1B** shows representative histograms of CFSE fluorescence
344 intensity (FL-1) of GL261 cells depicted in **Figure 1A**.

345 The effect of gedunin on cell viability was evaluated by the MTT assay. The incubation
346 of GL261 cells with gedunin decreased mitochondrial function in a concentration-
347 dependent manner within 24 and 72 h (**Fig. 1C**). MTT assay was also performed on
348 primary mixed glial cells to evaluate gedunin toxicity to non-tumoral cells. Gedunin
349 effect on primary mixed glial cells was less toxic, and higher concentrations were required
350 to induce cell death when compared to GL261 cells (**Fig. 1C**). The half-maximal
351 inhibitory concentration [IC50] of gedunin on GL261 cells was 2.3 times lower than the
352 IC_{50} observed on primary glial cells (**Fig. 1D**). Temozolomide, the first-line treatment for
353 glioblastoma, also reduced GL261 viability within 72 h in a concentration-dependent
354 manner (**Suppl. Fig. 1**). Considering the antiproliferative and cytotoxic effects of gedunin
355 on GL261 cells, we further examined whether this limonoid induced apoptosis.
356

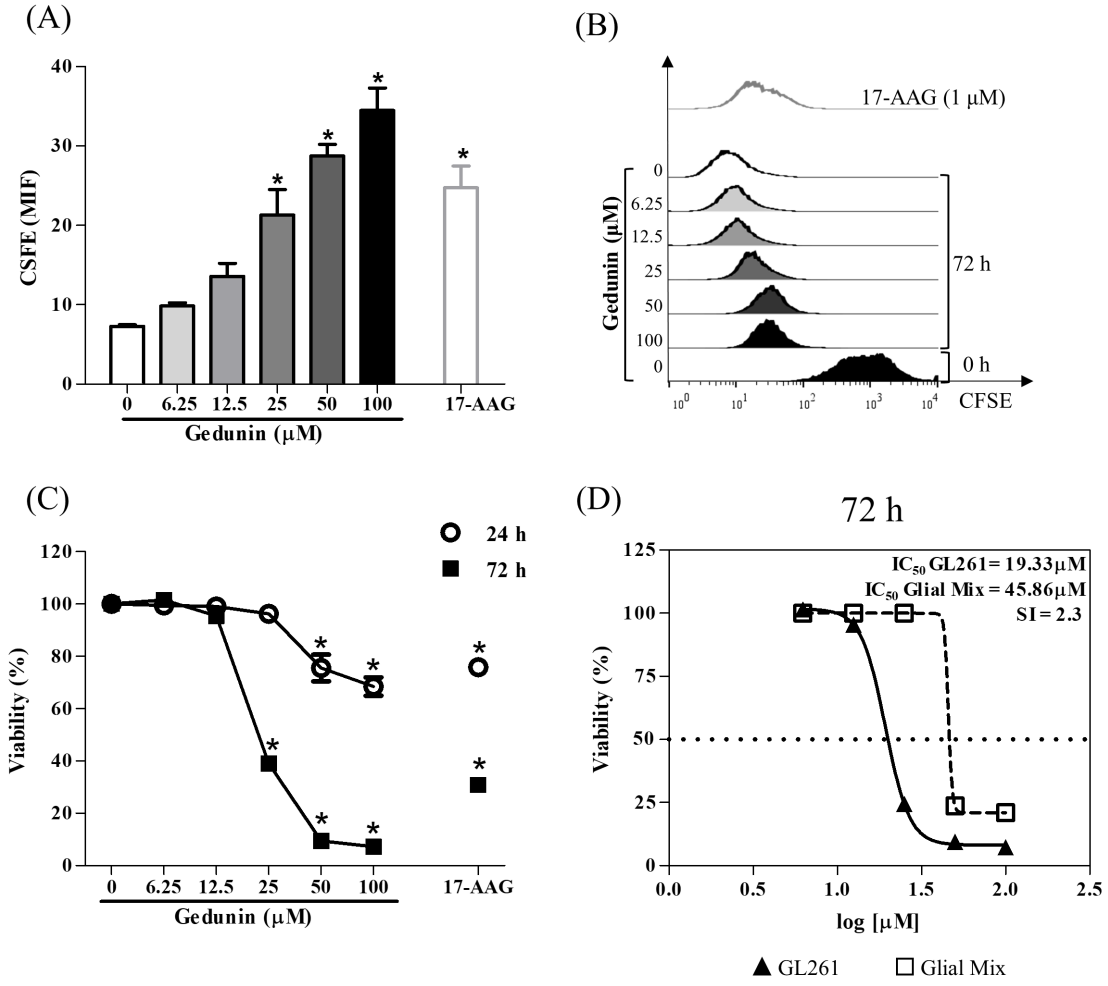

Figure 1. *Gedunin impairs GL261 cell proliferation.* (A) Effect of gedunin (6.25-100 μM) and 17-AAG (1 μM) on GL261 cell proliferation evaluated by CFSE staining and analyzed by FACScalibur (BD Biosciences) 72 h after incubation. Results are expressed as the mean ± SEM of median fluorescence intensity (MFI) from triplicate wells from three independent experiments. (B) Representative histogram shows CFSE fluorescence intensity (FL-1) from one experiment. (C) Effect of gedunin (6.25-100 μM) and 17-AAG (1 μM) on GL261 cell viability evaluated by MTT reduction assay (SpectraMax M5, Molecular Devices) 24 and 72 h after incubation. (D) IC50 values of gedunin treatment on GL261 and glial mixed cells 72 h after incubation. SI: selectivity index.

3.2 Gedunin induces GL261 cell apoptosis in vitro

Apoptosis is regulated by a series of signaling events that include disruption of the mitochondrial membrane and phosphatidylserine externalization [46,47]. Membrane

372 phosphatidylserine staining by annexin V-FITC revealed that gedunin induced apoptosis
373 of GL261 cells in a concentration- and time-dependent manner (**Fig. 2A**). Apoptosis was
374 detected 24 h after treatment, and surpassed 90 % within 72 h, at the highest
375 concentrations. Representative dot plots of PI^+ and annexin V^+ cells are shown in **Figure**
376 **2B**. Apoptotic cells are characterized by a reduced ability to scatter light either in forward
377 or right angle directions [48]. Indeed, GL261 cells incubated with gedunin diminished
378 FSC-H and increased SSC-H intensities, when compared to non-treated cells (**Fig. 2C**).
379 Representative dot-plots of the effect of 17-AAG (1 μM) on GL261 apoptosis (24 h and
380 72 h) is available on **Supplemental Figure 2**.
381

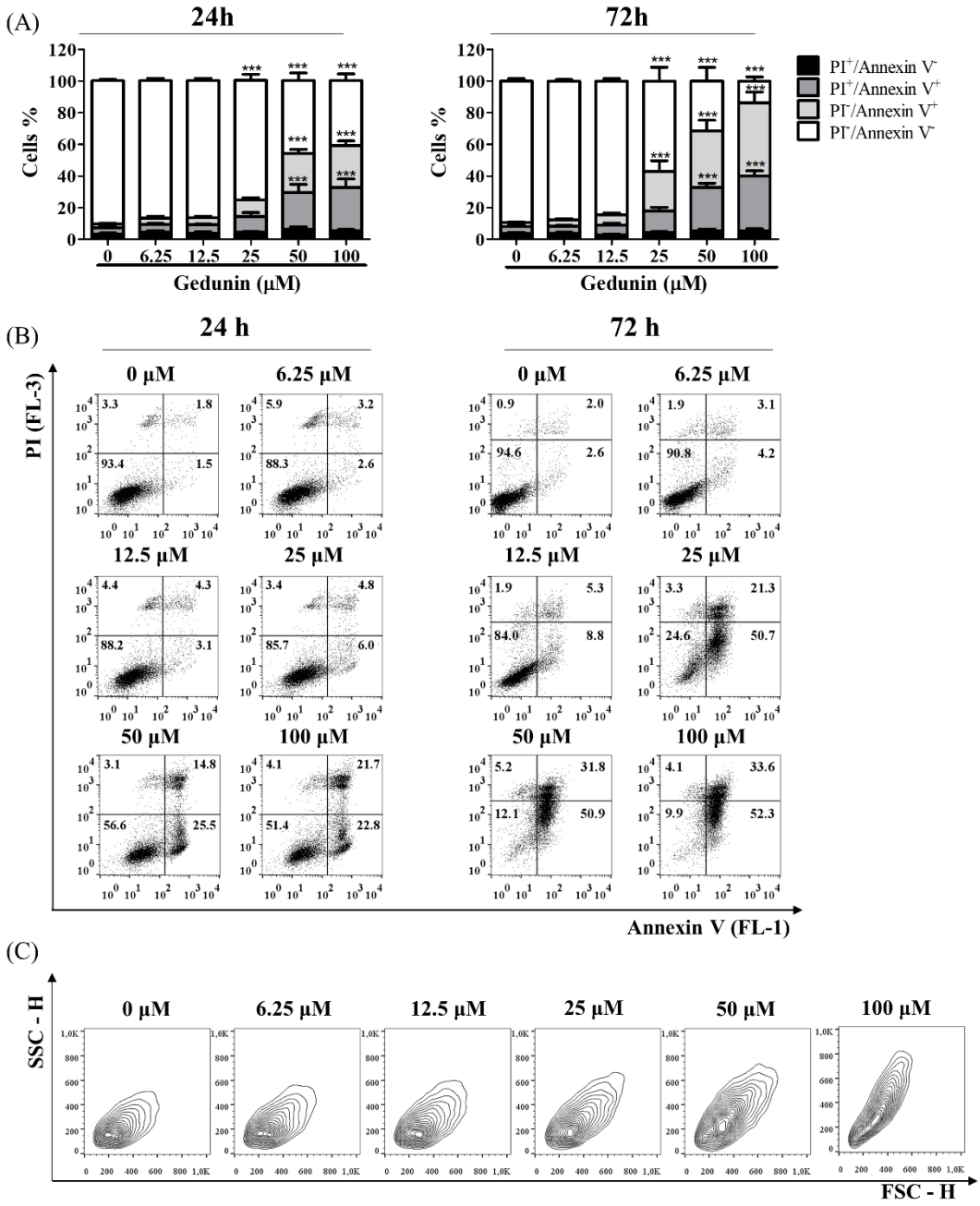

Figure 2. *Gedunin induces time- and concentration-dependent GL261 apoptosis.* (A) Effect of gedunin (6.25-100 µM) on GL261 cell (2×10^4/well) apoptosis evaluated by propidium iodide and annexin V-FITC staining MTT (FacsCalibur – BD Biosciences) 24 h and 72 h after incubation. Results are expressed as the mean ± SEM of viability percentage from triplicates wells from three independent experiments (24 well plates). * indicates statistically significant differences ($p \leq 0.05$) between treated and untreated cells. (B) Representative dot plots of flow cytometry analysis of gedunin-treated GL261 cells labeled with annexin V-FITC and PI after 24 and 72 h incubation. (C) Representative

391 contour plots of SSC-H and FSC-H of gedunin-treated (6.25 - 100 μM) GL261 cells after
392 72 h.
393

394 ***3.3 Gedunin impairs GL261 cell migration and invasiveness in vitro***

395 Tumor cell migration is an earlier step in cancer dissemination and invasion [49,50].
396 Scratch assay shows that gedunin (12.5 and 25 μM) reduced GL261 cell migration when
397 compared to the untreated group within 24 h, 48 h, and 72 h (**Fig. 3A, B**). Confirming
398 results obtained in the scratch assay, reduction of chemotaxis was also observed in the
399 Boyden chamber migration assay, in which gedunin treatment (25 μM) impaired cell
400 migration within 48 h (**Fig. 3C**).

401 Extracellular matrix remodeling by the proteolytic activity of tumor cell matrix
402 metalloproteinases (MMPs) is a crucial step for tumor cell invasion in the surrounding
403 tissue [51]. Gedunin also reduced the activity of MMP-2 (**Fig. 3D**), suggesting that this
404 limonoid impairs different mechanisms associated with tumor cell invasion. In addition,
405 we observed that gedunin treatment increased VEGF levels in the supernatant of GL261
406 cells (**Fig. 3E**), a phenomenon that does not contribute to its antitumoral effect since pro-
407 angiogenic mediators contribute to tumor cell metastasis [52,53].
408

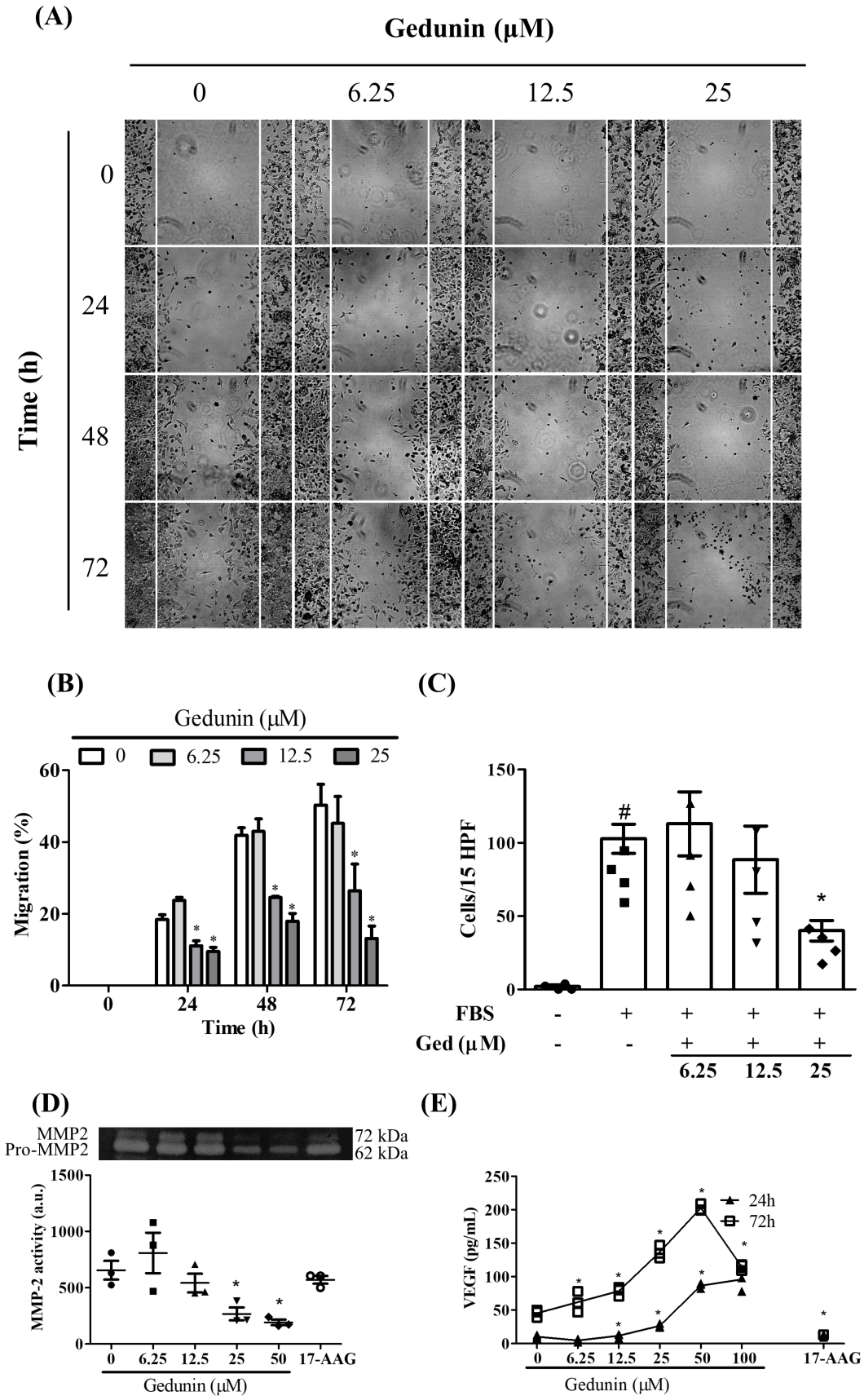
(A)
Gedunin (μM)
0
6.25
12.5
25
Time (h)
0
24
48
72
(B)
Gedunin (μM)
0
6.25
12.5
25
Migration (%)
Time (h)
(C)
Cells/15 HPF
FBS
Ged (μM)
6.25
12.5
25
(D)
MMP2
Pro-MMP2
72 kDa
62 kDa
MMP-2 activity (a.u.)
17-AAG
Gedunin (μM)
(E)
24h
72h
VEGF (pg/mL)
17-AAG
Gedunin (μM)

409

410 **Figure 3.** *Gedunin impairs in vitro GL261 cell migration and invasiveness.* (A)
411 Microscopic views of *in vitro* scratch assay. GL261 migration into the scratched area 24-
412 72 h after gedunin treatment (6.25-25 μM). (B) Percentages of GL261 cell migration
413 calculated as the ratio of uncovered area (24-72 h) by the initial scratched area (0 h).
414 Results are expressed as the mean ± SEM from two independent experiments (6 well
415 plates). (C) Boyden chamber chemotaxis assay demonstrating the number of gedunin-
416 treated or untreated cells per 15 high power fields (HPF) after 24 h migration. Results are
417 expressed as the mean ± SEM from quadruplicate wells. (D) MMP-2 activity of GL261
418 cell supernatant assessed by zymography assay 48 h after gedunin treatment (6.25-50
419 μM). Results are expressed as the mean ± SEM from two independent experiments. (E)
420 VEGF quantification (ng/mL) in cell supernatant by ELISA assay 24 and 72 h after
421 gedunin treatment (6.25-100 μM). * indicates statistically significant differences ($p \leq$
422 0.05) between treated and untreated cells, whereas # indicates statistically significant
423 differences ($p \leq 0.05$) between stimulated and unstimulated cells. FBS: fetal bovine
424 serum.
425

426 ***3.4 Gedunin modulates signaling proteins in GL261 cells***

427 Genomic characterization of glioblastoma frequently shows amplification and
428 phosphorylation of RTK (receptor tyrosine kinase), which ultimately leads to its
429 autoactivation and downstream signaling pathways, resulting in constitutive cell
430 proliferation and resistance to apoptosis [54]. PI3K/AKT and Ras/ERK are the main pro-
431 survival pathways triggered by RTK activation in glioblastoma cells [55–57]. **Figure 4A-**
432 **E** illustrates the effect of gedunin in these pathways in *in vitro*-treated GL261 cells.

433 Gedunin treatment reduced the amount of total cell protein within 24 h, as shown in
434 representative immunoblots of proliferating cell nuclear antigen (PCNA) content from 8
435 independent experiments (**Fig. 4A**; replicates in **Suppl. Fig. 3**). Immunostaining of total
436 proteins also decreased in gedunin-treated cells (**Fig. 4A**), which may be explained by the
437 induction of apoptosis and cell death.

438 When the measurements were normalized by the constitutive protein, PCNA, no specific
439 reduction of total STAT3 or total ERK 1/2 was observed after gedunin treatment (**Fig.**
440 **4B, C**). Total AKT protein content was reduced in GL261 cells treated with gedunin (50
441 μM), when compared to untreated cell values (**Fig. 4D)**.

442 Phosphorylation of STAT3 (**Fig. 4E**) and ERK 1/2 (**Fig. 4F**) was induced by gedunin.
443 These results suggest that apoptosis driven by gedunin is followed by a compensatory

444 activation/phosphorylation of these survival pathways. The treatment with 17-AAG also
445 reduced total protein content but did not induce this putative compensatory activation of
446 STAT3 and ERK pathways within the 24 h incubation. Even though the mean of
447 phosphorylated AKT (pAKT) increased in gedunin-treated cells (**Fig. 4C**), it was not
448 significantly different from untreated cells (**Fig. 4G**).
449

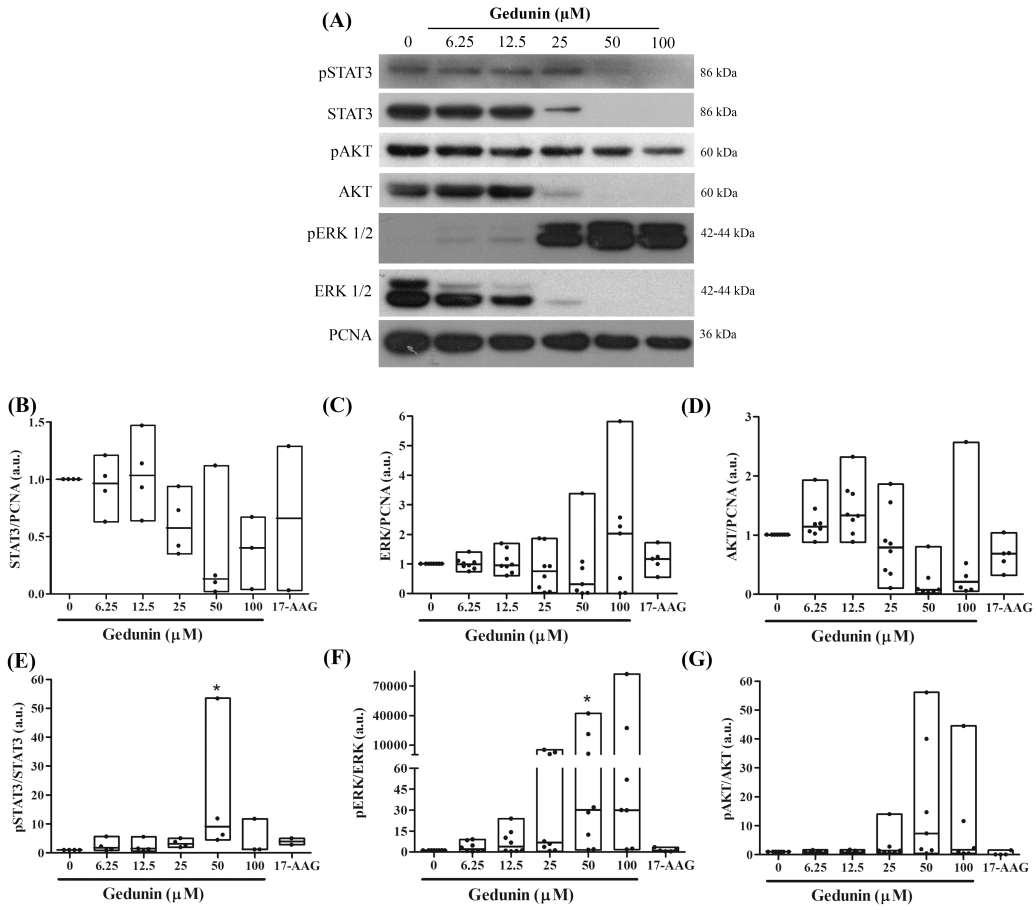

450

451 **Figure 4.** *Gedunin activates PI3K/AKT and STAT3/ERK 1/2 pathways.* Western blot
452 analysis of the effect of gedunin (6.25 – 100 μM) on intracellular signaling proteins, 24 h
453 after treatment. (A) Representative immunoblots of one experiment out of 8 independent
454 experiments with a similar trend. Box plots of (B) STAT3/PCNA, (C) ERK/PCNA, (D)
455 AKT/PCNA, (E) pSTAT3/STAT3, (F) pERK/ERK, (G) pAKT/AKT intracellular
456 signaling pathways on GL261 cells. 17-AAG was used as the reference control of HSP90
457 activity inhibition. PCNA was used as the loading control. Results are expressed as the
458 mean ± SEM of protein expression from eight independent experiments. * indicates
459 statistically significant differences ($p \leq 0.05$) between treated and untreated cells, whereas

460 # indicates statistically significant differences ($p \leq 0.05$) between treated and untreated
461 cells. Please find the uncropped blots at the supplemental figure 3.
462

463 ***3.5 Gedunin effect on glioblastoma in vivo***

464 The orthotopic C57BL/6 mouse glioblastoma model used in the present study has been
465 established as a standard procedure to reproduce human molecular and histological
466 features of glioblastoma [58,59]. Biodistribution data obtained by our group show that
467 ^{99m}Tc-labeled-gedunin did not reach substantial levels in the brain tissue when
468 intravenously injected in mice (Costa et al., *manuscript in preparation*). We, therefore,
469 assessed whether gedunin *in vivo* treatment was effective by using osmotic pumps placed
470 *in situ.*

471 Computed tomography (CT) scans revealed solid tumor growth that occupied an
472 extensive area of the brain tissue of mice from all groups (white mass, top panels in
473 black background of **Fig. 5A,** indicated by an asterisk in the upper left image scan).
474 Three-dimensional reconstructions of CT images are shown in **Figure 5** bottom panels,
475 in which tumor mass is represented by white over gray (brain) areas. Even though tumor
476 volume median values (mm^3) of gedunin-treated mice were smaller than those for
477 untreated or DMSO-injected mice, variability within groups was high (lowest and
478 highest tumor volume values for each group were: untreated, 21.7 - 75.6; DMSO, 16.8 -
479 83.6; GED, 11.7 - 67.4). No significant differences were observed between groups
480 (ANOVA, $p = 0.106$; **Fig. 5B, C**). **Supplemental Figure 4** shows CT of mouse brains
481 with and without tumors, for a better illustration of the tumor mass. Body mass (g) was
482 measured before GL261 injection and 28 days later and no alterations were observed
483 (data not shown).

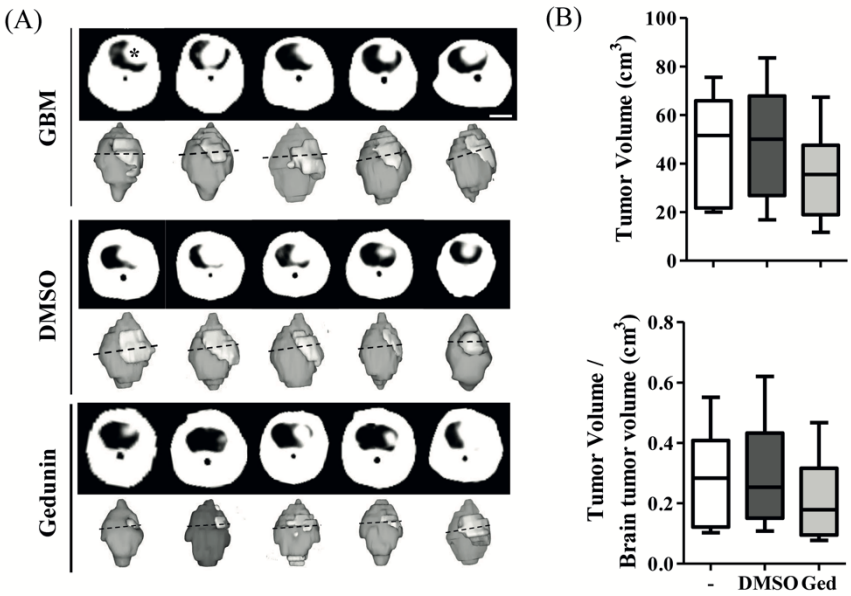

Figure 5. *Brain CT analysis of gedunin-treated mice.* (A) Representative sequential coronal CT-images and respective 3D brain reconstructions (dorsal view) from untreated, DMSO-injected and gedunin (250 μM)-treated mice. Lighter regions in 3D reconstructions represent brain tumors. Images were acquired after 14-day *in situ* treatment (Alzet® osmotic minipumps) in GL261 cell-injected mice (1×10^5 cells/brain/2 μL). Boxplot graphs show the ratio between tumor and mouse brain volume values (B) and tumor volume values (C) from 6-8 mice per group out of 2 independent experiments. Tumor volumetry was determined by selecting contrast-enhanced regions of interest in coronal sections using InVesalius 3.1.1 software. CT: computed tomography. *White area corresponds to glioblastoma observed in all CT scans. Dashed line: coronal slice cut point.

Histological examination of coronal brain sections of untreated, DMSO- and gedunin-treated groups revealed that even though gedunin-treated mice had larger tumor-induced lesion areas, they displayed reduced vascular structures (**Table 1**). Areas of liquefactive necrosis, intratumoral hemorrhage, and mitosis were not statistically different between groups. **Figure 6** depicts representative images of GL261-injected mouse coronal brain slices stained with hematoxylin and eosin 28 days after injections. **Figure 6 (A-C)** insets represent 400× magnification of intratumoral perinecrotic regions, in which liquefactive necrosis can be observed by white spaces within the glioblastoma tissue, resulting in the loss of tissue architecture. **Figure 6 (D-F)** displays 1000 × magnification of representative images of tumor tissue showing mitosis, characterized by tumor cell proliferation, and areas of hemorrhage, defined by the presence of red blood cells.

507

508 **Table 1**. **Glioblastoma histology features after gedunin *in vivo* treatment**

	Untreated	DMSO	Gedunin	p
Lesion size	27%	45%	45.2%	NS
Vascular Structures	13	32	8	P< 0.05 *
Liquefactive Necrosis	9.6%	10.6%	8.8%	NS
Intratumoral Hemorrhage	+	++	++	NS
Mitosis	+	++	+	NS

509 **Table 1**. *Glioblastoma histology features after gedunin in vivo treatment.* Table shows absolute
510 and semi-quantitative description of the histological analyses of brain slices and p-values of
511 gedunin-treated vs DMSO-treated mice, analyzed by Tukey's post-test. NS= non-significant; +=
512 discrete; ++= moderate.
513

514

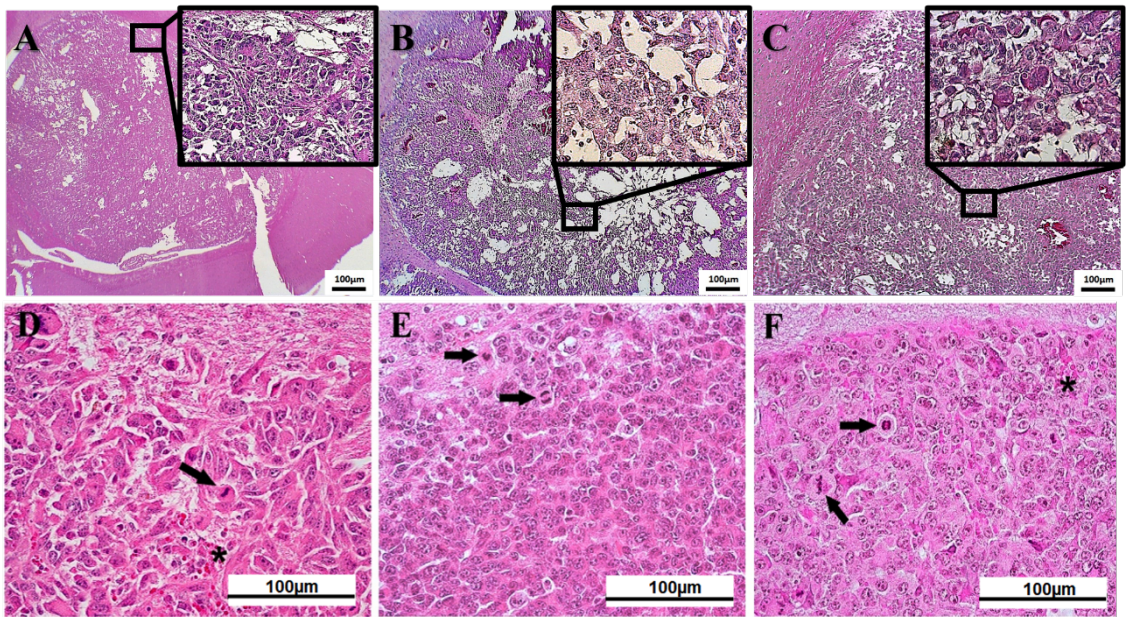

515

516

517 **Figure 6.** *Histological analysis of gedunin-treated mice.* Representative images of
518 coronal brain slices from stained with hematoxylin and eosin 28 days after GL261 cell
519 implantation of untreated (A,D), DMSO- (B,E), and gedunin-treated (C,F) mice (n=8 per
520 group). Upper panels (A-C) depict low magnification images (40 ×) of the extent of the
521 tumor area for each experimental group. Corresponding high-magnification insets (400
522 ×) of intratumoral perinecrotic regions show liquefactive necrosis (white regions). Lower
523 panels (D-F), high magnification images (1000 ×) from the same animals in (A-C), show
524 mitosis (black arrows) and areas of hemorrhage (asterisks) in intratumoral regions.
525

526

527 ***4. Discussion***

528 Uncontrolled proliferation and apoptosis resistance are central features of tumor
529 development, being major targets for cancer treatment [17]. HSP90 is a key factor for
530 tumor growth, since it chaperones several essential proteins involved in oncogenic
531 processes. In the present study, we demonstrate that gedunin, a natural occurring HSP90
532 inhibitor, impairs glioblastoma cell growth *in vitro*, by arresting proliferation and
533 inducing cell death in non-toxic concentrations to primary brain cells. Gedunin also
534 reduced glioblastoma cell migration, tumor-related signaling pathways, and extracellular
535 metalloproteinase MMP-2 activity, features involved in glioblastoma growth. GL261-
536 orthotopically injected C57BL/6 mice treated with gedunin showed reduced presence of
537 vascular structures, even though no changes were observed in tumor-size.

538 Data shown in **Supplemental Figure 5** supports previous knowledge that both gedunin
539 and other HSP90-binding agents induce the expression of HSP70 in cancer cells due to
540 HSP90 inhibition [60–62]. The antiproliferative and cytotoxic effects of gedunin on
541 GL261 cells are also in accordance with previous *in vitro* results showing similar
542 antitumoral effects of gedunin against different cell lines [35,37–40]. Worthy of note,
543 gedunin toxicity against GL261 cells was achieved at a concentration lower than half the
544 one required to affect primary glial cells, with a selectivity index of 2.3 [63]. This might
545 be explained by the increased affinity of HSP90 inhibitors to HSP90 machinery expressed
546 by tumor cells [16], or by biological and metabolic differences between primary and
547 glioblastoma cells [64]. Gedunin-triggered apoptosis, detected by phosphatidylserine
548 exposure on the cell surface, was confirmed by flow cytometric analysis of cell physical
549 criteria that showed the reduced size and increased granularity of apoptotic cells, due to
550 the formation of apoptotic bodies and plasma membrane blebbing [48]. Our results clearly
551 show that, as apoptosis progresses, GL261 cell FSC becomes progressively lower, likely
552 due to cell dehydration and shrinkage. On the other hand, enhancement of SSC occurs
553 due to cytoplasm and nuclear condensation [48,65].

554 Glioblastoma is a highly invasive and diffuse tumor that requires cell migration and
555 extracellular matrix degradation to spread to adjacent tissue [66,67]. Scratch and
556 chemotaxis assays showed that gedunin diminished GL261 migration, in concentrations
557 and time points lower than the ones that induced cytotoxicity. Another way by which

558 gedunin controls tumor invasiveness is by inhibiting MMP-2 activity, with a higher effect
559 than 17-AAG. Indeed, it has been shown that HSP90 stabilizes and promotes the
560 activation of extracellular MMP-2, being crucial for GL261 and HT-1080 tumor cell
561 invasion [68,69].

562 Our results show that gedunin induced a reduction of total protein in GL261 cells, which
563 is compatible with the HSP90 inhibition. PI3K/AKT and STAT3 are signaling pathways
564 that function as pro-survival factors in a wide range of primary tumors, including
565 glioblastoma [55,70]. Reduced expression of total PI3K and AKT by gedunin suggests
566 that this limonoid impairs either PI3K/AKT network or an upstream protein, such as
567 epithelial growth factor receptor (EGFR). In accordance, it has been shown that gedunin
568 also impaired the PI3K/AKT/mTOR pathway in *in vivo* models of hamster oral carcinoma
569 [40] and murine pancreatic cancer [37]. Even though PI3K/AKT is the preferential
570 signaling pathway in glioblastoma, it has been reported that glioblastoma cells are not
571 exclusively dependent on this pathway and that PI3K/AKT/mTOR-specific inhibitors
572 might not be effective against this brain tumor [55]. Hence, we evaluated the effect of
573 gedunin in AKT, ERK 1/2, and STAT3 signaling, which are also altered in glioblastoma
574 cells and are involved in the cell cycle [71,72]. It is important to note that even though
575 gedunin treatment reduced total ERK content, it did not inhibit ERK1/2 phosphorylation.
576 On the contrary, ERK was strongly phosphorylated/activated in cells treated with
577 gedunin. Indeed, Duron et al. showed that HSP90 inhibition can also prompt the
578 phosphorylation/activation of ERK [73,74]. There might be a compensatory survival
579 mechanism in GL261 cells that activate ERK when HSP90 is inhibited. This result must
580 be further explored and points to the perspective of combining gedunin with ERK
581 inhibitor anti-tumoral drugs.

582 It has been previously reported in glioblastoma that constitutive activation of STAT3
583 results from the fusion of the RTK epidermal growth factor receptor (EGFR) with the
584 GTP-binding protein Septin 14 (SEPT14) [57]. STAT3 signaling promotes glioblastoma
585 cell survival, and suppresses apoptosis [57]. Abnormal STAT3 activation in glioblastoma
586 is correlated with the control of a number of events involved in tumor growth [70]. The
587 late (24 h) activation of STAT3 by gedunin might also correspond to survival feedback
588 following the induction of apoptosis. Therefore, gedunin may inhibit GL261 cell
589 proliferation by acting on different pathways that induce apoptosis. Activation of STAT3

590 is required for VEGF production [75,76]. Even though we observed that gedunin impaired
591 signaling pathways (which was expected to impair both VEGF synthesis and signaling
592 pathway), this phenomenon did not inhibit VEGF release by GL261 *in vitro*.

593 As previously mentioned in the results section, even though our findings indicate that
594 gedunin fits the predicted ADMET criteria for druggability and BBB permeation,
595 systemic (i.v.) administration of ^{99m}TC-labeled gedunin failed to reach the brain tissue at
596 substantial levels (Costa *et al*., manuscript in preparation). Hence, we used gedunin-filled
597 Alzet® minipumps to perform *in situ* treatment (resembling the FDA-approved Gliadel®
598 [carmustine] implants) to ensure that gedunin would be available at the tumor site. It is
599 important to note that the residual volume of gedunin inside the minipumps was measured
600 at the end of treatment to ensure that gedunin was released *in situ*, (values shown in
601 **Suppl. Table 1**). We observed that the number of mice bearing reduced-volume tumors
602 was higher in gedunin-treated group when compared to DMSO-treated group, even
603 though this treatment did not significantly reduce tumor volumes detected by CT imaging.
604 Regarding our CT imaging results, it is important to emphasize the limitation of the
605 technique, since the limited spatial resolution of clinical CT scanners might not be precise
606 to analyze such a small brain [77,78]. While our findings reinforce the feasibility of using
607 clinical CT scanners for *in vivo* brain tumor imaging in mice, their use for detecting
608 treatment responses in tumor volume requires further investigation, since clinical CT
609 scans are made for imaging humans that have brain volumes roughly 3,000 times greater
610 than mice [79–81]. Another limitation is that mouse tumor sizes were not evaluated over
611 the days, since CT scan was only feasible in mice with no minipump implants, due to the
612 stainless steel of brain infusion cannulas.
613 As expected, GL261-injections triggered the development of mouse glioblastoma in
614 orthotopically-injected C57BL/6 mouse with liquefactive necrosis, hemorrhage, mitosis
615 and increased vascular structures [59]. *In situ* treatment with gedunin reduced the
616 presence of vascular structures, which might decrease tumor nutritional supply.
617 Considering that gedunin increased the production of VEGF *in vitro*, this finding might
618 suggest that gedunin impairs angiogenesis in GL261 tumors by a mechanism
619 independent of VEGF *in vivo* as previously described [82]. Despite the reduction of
620 vascular structures, there was no evidence of reduction in tumor size. Moreover, the
621 impact of the reduction in vascular structures on the survival rate of orthotopically-

622 injected C57BL/6 mice was not evaluated. Therefore, whether gedunin *in vivo* treatment
623 impairs mouse glioblastoma growth needs to be further investigated, including *in situ*
624 measurement of gedunin release from minipumps and VEGF contents. Noteworthy, both
625 DMSO- and gedunin-treated mice showed increased lesion areas when compared to
626 untreated mice, which might be a consequence of the surgical procedure required for
627 minipump implantation. It is possible that an optimized treatment protocol including a
628 postoperative treatment (as generally performed in glioblastoma patients) and/or
629 association with other drugs result in a better outcome.

630 The severity and the poor prognosis of patients bearing glioblastoma urge for new
631 therapeutical targets and drugs. Data presented in this paper sheds light on alternative
632 treatments for this type of tumor by revealing GL261 dependency of HSP90 and gedunin
633 as a potential lead compound.
634

635 ***Author contributions***

636 CP, TEMMC, and TEK conceived and designed the work. TEMMC, CP, TEK, ACM,
637 and MGH designed experiments. TEMMC, TAP, LNS, EMC, CCF, CMMM, JXP, VGR,
638 and TEK performed the experiments, acquired, and/or analyzed data. CP, TEK, ACM,
639 YAV, JXC, and MGH contributed with funding and resources. CP supervised the work.
640 CP and TEMMC wrote the original draft. CMMM and TEK wrote and revised the
641 manuscript. All authors revised and edited the final manuscript.

642

643 ***Acknowledgments***

644 The authors gratefully acknowledge Dr. André Luis Peixoto Candéa, D.Sc. Erika Tatiana
645 Muñoz, Dr. Samara Cristina Ferreira Machado, Edson Santos Silva, Filipe Leal Portilho,
646 Ubirajara Ribeiro, and Maria Heloisa Oliveira for technical support. We also thank the
647 Institute for Biomodels Science and Technology (Fiocruz) for providing mice, and the
648 Center for Cancer Control (CUCC, UERJ) for the help with CT imaging acquisition.
649

650 ***Funding***

651 This work was supported by the Carlos Chagas Filho Research Support Foundation
652 (FAPERJ), the Coordination for the Improvement of Higher Education Personnel

(CAPES), the Brazilian agency National Council for Scientific and Technological Development (CNPq), and the Oswaldo Cruz Foundation (Fiocruz). CP, MGMO, and ACM hold fellowships from CNPq. TEMMC was a PhD student from the Graduate Program in Cell and Molecular Biology (IOC/Fiocruz).

Conflict of interest

The authors declare no conflict of interest.

References

[1] D.N. Louis, A. Perry, G. Reifenberger, A. von Deimling, D. Figarella-Branger, W.K. Cavenee, H. Ohgaki, O.D. Wiestler, P. Kleihues, D.W. Ellison, The 2016 World Health Organization Classification of Tumors of the Central Nervous System: a summary, Acta Neuropathol. 131 (2016) 803–820. doi:10.1007/s00401-016-1545-1.

[2] Q.T. Ostrom, M. Price, C. Neff, G. Cioffi, K.A. Waite, C. Kruchko, J.S. Barnholtz-Sloan, CBTRUS Statistical Report: Primary Brain and Other Central Nervous System Tumors Diagnosed in the United States in 2015–2019, Neuro. Oncol. 24 (2022) v1–v95. doi:10.1093/neuonc/noac202.

[3] P.D. Delgado-López, E.M. Corrales-García, Survival in glioblastoma: a review on the impact of treatment modalities, Clin Transl Oncol. 18 (2016) 1062–1071. doi:10.1007/s12094-016-1497-x.

[4] R. Stupp, W.P. Mason, M.J. van den Bent, M. Weller, B. Fisher, M.J. Taphoorn, K. Belanger, A.A. Brandes, C. Marosi, U. Bogdahn, J. Curschmann, R.C. Janzer, S.K. Ludwin, T. Gorlia, A. Allgeier, D. Lacombe, J.G. Cairncross, E. Eisenhauer, R.O. Mirimanoff, E.O. for R. Groups, T. of Cancer Brain Tumor, Radiotherapy, N.C.I. of C.C.T. Group, Radiotherapy plus concomitant and adjuvant temozolomide for glioblastoma, N Engl J Med. 352 (2005) 987–996. doi:10.1056/NEJMoa043330.

[5] M. Niewald, C. Berdel, J. Fleckenstein, N. Licht, R. Ketter, C. Rübe, Toxicity after radiochemotherapy for glioblastoma using temozolomide - a retrospective evaluation, Radiat. Oncol. 6 (2011) 141. doi:10.1186/1748-717X-6-141.

[6] J. Dinnes, C. Cave, S. Huang, R. Milne, A rapid and systematic review of the

effectiveness of temozolomide for the treatment of recurrent malignant glioma, Br. J. Cancer. 86 (2002) 501–505. doi:10.1038/sj.bjc.6600135.

[7] F. Attarian, F. Taghizadeh-Hesary, A. Fanipakdel, S.A. Javadinia, P. Porouhan, B. PeyroShabany, D. Fazilat-Panah, A Systematic Review and Meta-Analysis on the Number of Adjuvant Temozolomide Cycles in Newly Diagnosed Glioblastoma, Front. Oncol. 11 (2021) 1–6. doi:10.3389/fonc.2021.779491.

[8] E. Lechapt-Zalcman, G. Levallet, A.E. Dugué, A. Vital, M.-D. Diebold, P. Menei, P. Colin, P. Peruzzy, E. Emery, M. Bernaudin, F. Chapon, J.-S. Guillamo, O6-methylguanine-DNA methyltransferase (MGMT) promoter methylation and low MGMT-encoded protein expression as prognostic markers in glioblastoma patients treated with biodegradable carmustine wafer implants after initial surgery followed by radiotherapy w, Cancer. 118 (2012) 4545–4554. doi:https://doi.org/10.1002/cncr.27441.

[9] L. Jena, E. McErlean, H. McCarthy, Delivery across the blood-brain barrier: nanomedicine for glioblastoma multiforme, Drug Deliv. Transl. Res. 10 (2020) 304–318. doi:10.1007/s13346-019-00679-2.

[10] M.J. McGirt, K.D. Than, J.D. Weingart, K.L. Chaichana, F.J. Attenello, A. Olivi, J. Laterra, L.R. Kleinberg, S.A. Grossman, H. Brem, A. Quiñones-Hinojosa, Gliadel (BCNU) wafer plus concomitant temozolomide therapy after primary resection of glioblastoma multiforme, J. Neurosurg. JNS. 110 (2009) 583–588. doi:10.3171/2008.5.17557.

[11] Z. Qi, W. Xing, C. Shao, C. Yang, Z. Wang, The role of Gliadel wafers in the treatment of newly diagnosed GBM: a meta-analysis, Drug Des. Devel. Ther. 9 (2015) 3341. doi:10.2147/DDDT.S85943.

[12] T. Reithmeier, E. Graf, T. Piroth, M. Trippel, M.O. Pinsker, G. Nikkhah, BCNU for recurrent glioblastoma multiforme: efficacy, toxicity and prognostic factors, BMC Cancer. 10 (2010) 30. doi:10.1186/1471-2407-10-30.

[13] A. Bregy, A.H. Shah, M. V Diaz, H.E. Pierce, P.L. Ames, D. Diaz, R.J. Komotar, The role of Gliadel wafers in the treatment of high-grade gliomas, Expert Rev. Anticancer Ther. 13 (2013) 1453–1461. doi:10.1586/14737140.2013.840090.

[14] O. Alexandru, S. Purcaru, L. Tataranu, L. Lucan, J. Castro, C. Folcuţi, S.-A. Artene, C. Tuţă, A. Dricu, The Influence of EGFR Inactivation on the Radiation

718 Response in High Grade Glioma, Int. J. Mol. Sci. 19 (2018) 229.
719 doi:10.3390/ijms19010229.
720 [15] S. Tanaka, D.N. Louis, W.T. Curry, T.T. Batchelor, J. Dietrich, Diagnostic and
721 therapeutic avenues for glioblastoma: no longer a dead end?, Nat. Rev. Clin.
722 Oncol. 10 (2013) 14–26. doi:10.1038/nrclinonc.2012.204.
723 [16] J. Trepel, M. Mollapour, G. Giaccone, L. Neckers, Targeting the dynamic HSP90
724 complex in cancer, Nat Rev Cancer. 10 (2010) 537–549. doi:10.1038/nrc2887.
725 [17] D. Hanahan, R.A. Weinberg, Hallmarks of cancer: the next generation, Cell. 144
726 (2011) 646–674. doi:10.1016/j.cell.2011.02.013.
727 [18] Q. Cheng, J.T. Chang, J. Geradts, L.M. Neckers, T. Haystead, N.L. Spector, H.K.
728 Lyerly, Amplification and high-level expression of heat shock protein 90 marks
729 aggressive phenotypes of human epidermal growth factor receptor 2 negative
730 breast cancer, Breast Cancer Res. 14 (2012) R62. doi:10.1186/bcr3168.
731 [19] H. Kubota, S. Yamamoto, E. Itoh, Y. Abe, A. Nakamura, Y. Izumi, H. Okada, M.
732 Iida, H. Nanjo, H. Itoh, Y. Yamamoto, Increased expression of co-chaperone
733 HOP with HSP90 and HSC70 and complex formation in human colonic
734 carcinoma, Cell Stress Chaperones. 15 (2010) 1003–1011. doi:10.1007/s12192-
735 010-0211-0.
736 [20] M.M. McCarthy, E. Pick, Y. Kluger, B. Gould-Rothberg, R. Lazova, R.L. Camp,
737 D.L. Rimm, H.M. Kluger, HSP90 as a marker of progression in melanoma, Ann
738 Oncol. 19 (2008) 590–594. doi:10.1093/annonc/mdm545.
739 [21] E. Pick, Y. Kluger, J.M. Giltnane, C. Moeder, R.L. Camp, D.L. Rimm, H.M.
740 Kluger, High HSP90 expression is associated with decreased survival in breast
741 cancer, Cancer Res. 67 (2007) 2932–2937. doi:10.1158/0008-5472.CAN-06-
742 4511.
743 [22] F.H. Schopf, M.M. Biebl, J. Buchner, The HSP90 chaperone machinery, Nat Rev
744 Mol Cell Biol. 18 (2017) 345–360. doi:10.1038/nrm.2017.20.
745 [23] Y. Fukuyo, C.R. Hunt, N. Horikoshi, Geldanamycin and its anti-cancer activities,
746 Cancer Lett. 290 (2010) 24–35. doi:10.1016/j.canlet.2009.07.010.
747 [24] M. V Blagosklonny, Hsp-90-associated oncoproteins: multiple targets of
748 geldanamycin and its analogs, Leukemia. 16 (2002) 455–462.
749 doi:10.1038/sj.leu.2402415.

750 [25] N. Gaspar, S.Y. Sharp, S.A. Eccles, S. Gowan, S. Popov, C. Jones, A. Pearson,
751 G. Vassal, P. Workman, Mechanistic evaluation of the novel HSP90 inhibitor
752 NVP-AUY922 in adult and pediatric glioblastoma, Mol. Cancer Ther. 9 (2010)
753 1219–1233. doi:10.1158/1535-7163.MCT-09-0683.
754 [26] B. Newman, Y. Liu, H.F. Lee, D. Sun, Y. Wang, HSP90 inhibitor 17-AAG
755 selectively eradicates lymphoma stem cells, Cancer Res. 72 (2012) 4551–4561.
756 doi:10.1158/0008-5472.CAN-11-3600.
757 [27] S.A. Eccles, A. Massey, F.I. Raynaud, S.Y. Sharp, G. Box, M. Valenti, L.
758 Patterson, A. de Haven Brandon, S. Gowan, F. Boxall, W. Aherne, M. Rowlands,
759 A. Hayes, V. Martins, F. Urban, K. Boxall, C. Prodromou, L. Pearl, K. James,
760 T.P. Matthews, K.M. Cheung, A. Kalusa, K. Jones, E. McDonald, X. Barril, P.A.
761 Brough, J.E. Cansfield, B. Dymock, M.J. Drysdale, H. Finch, R. Howes, R.E.
762 Hubbard, A. Surgenor, P. Webb, M. Wood, L. Wright, P. Workman, NVP-
763 AUY922: a novel heat shock protein 90 inhibitor active against xenograft tumor
764 growth, angiogenesis, and metastasis, Cancer Res. 68 (2008) 2850–2860.
765 doi:10.1158/0008-5472.CAN-07-5256.
766 [28] H.B. Kim, S.H. Lee, J.H. Um, W.K. Oh, D.W. Kim, C.D. Kang, S.H. Kim,
767 Sensitization of multidrug-resistant human cancer cells to Hsp90 inhibitors by
768 down-regulation of SIRT1, Oncotarget. 6 (2015) 36202–36218.
769 doi:10.18632/oncotarget.5343.
770 [29] T. Shimamura, S.A. Perera, K.P. Foley, J. Sang, S.J. Rodig, T. Inoue, L. Chen, D.
771 Li, J. Carretero, Y.C. Li, P. Sinha, C.D. Carey, C.L. Borgman, J.P. Jimenez, M.
772 Meyerson, W. Ying, J. Barsoum, K.K. Wong, G.I. Shapiro, I. Geoffrey,
773 Ganetespib (STA-9090), a nongeldanamycin HSP90 inhibitor, has potent
774 antitumor activity in in vitro and in vivo models of non-small cell lung cancer,
775 Clin Cancer Res. 18 (2012) 4973–4985. doi:10.1158/1078-0432.CCR-11-2967.
776 [30] Clinical Trials, (2020).
777 https://clinicaltrials.gov/ct2/results?cond=Cancer&term=HSP90+inhibitor&cntry
778 =&state=&city=&dist=.
779 [31] D.B. Solit, S.P. Ivy, C. Kopil, R. Sikorski, M.J. Morris, S.F. Slovin, W.K. Kelly,
780 A. Delacruz, T. Curley, G. Heller, S. Larson, L. Schwartz, M.J. Egorin, N.
781 Rosen, H.I. Scher, Cancer Therapy : Clinical Phase I T rial of 17-Allylamino-17-

782 Demethoxygeldanamycin in Patients with Advanced Cancer, 13 (2007) 1775–
783 1782. doi:10.1158/1078-0432.CCR-06-1863.
784 [32] D. Zhou, Y. Liu, J. Ye, W. Ying, L.S. Ogawa, T. Inoue, N. Tatsuta, Y. Wada, K.
785 Koya, Q. Huang, R.C. Bates, A.J. Sonderfan, A rat retinal damage model predicts
786 for potential clinical visual disturbances induced by Hsp90 inhibitors, Toxicol
787 Appl Pharmacol. 273 (2013) 401–409. doi:10.1016/j.taap.2013.09.018.
788 [33] G. Hallur, A. Sivramakrishnan, S. V Bhat, Three New Tetranortriterpenoids from
789 Neem Seed Oil, J. Nat. Prod. 65 (2002) 1177–1179. doi:10.1021/np0105174.
790 [34] G.E. Brandt, M.D. Schmidt, T.E. Prisinzano, B.S. Blagg, Gedunin, a novel hsp90
791 inhibitor: semisynthesis of derivatives and preliminary structure-activity
792 relationships, J Med Chem. 51 (2008) 6495–6502. doi:10.1021/jm8007486.
793 [35] C.A. Patwardhan, A. Fauq, L.B. Peterson, C. Miller, B.S. Blagg, A. Chadli,
794 Gedunin inactivates the co-chaperone p23 protein causing cancer cell death by
795 apoptosis, J Biol Chem. 288 (2013) 7313–7325. doi:10.1074/jbc.M112.427328.
796 [36] R.L. Matts, G.E. Brandt, Y. Lu, A. Dixit, M. Mollapour, S. Wang, A.C.
797 Donnelly, L. Neckers, G. Verkhivker, B.S. Blagg, A systematic protocol for the
798 characterization of Hsp90 modulators, Bioorg Med Chem. 19 (2011) 684–692.
799 doi:10.1016/j.bmc.2010.10.029.
800 [37] R. Subramani, E. Gonzalez, S.B. Nandy, A. Arumugam, F. Camacho, J. Medel,
801 D. Alabi, R. Lakshmanaswamy, Gedunin inhibits pancreatic cancer by altering
802 sonic hedgehog signaling pathway, Oncotarget. 8 (2017) 10891–10904.
803 doi:10.18632/oncotarget.8055.
804 [38] S.G. Kamath, N. Chen, Y. Xiong, R. Wenham, S. Apte, M. Humphrey, J.
805 Cragun, J.M. Lancaster, Gedunin, a novel natural substance, inhibits ovarian
806 cancer cell proliferation, Int J Gynecol Cancer. 19 (2009) 1564–1569.
807 doi:10.1111/IGC.0b013e3181a83135.
808 [39] S.J. Uddin, L. Nahar, J.A. Shilpi, M. Shoeb, T. Borkowski, S. Gibbons, M.
809 Middleton, M. Byres, S.D. Sarker, Gedunin, a limonoid from Xylocarpus
810 granatum, inhibits the growth of CaCo-2 colon cancer cell line in vitro, Phytother
811 Res. 21 (2007) 757–761. doi:10.1002/ptr.2159.
812 [40] K.K. Kishore T, R. Ganugula, D.R. Gade, G.B. Reddy, S. Nagini, Gedunin
813 abrogates aldose reductase, PI3K/Akt/mToR, and NF-κB signaling pathways to

814 inhibit angiogenesis in a hamster model of oral carcinogenesis, Tumour Biol. 37
815 (2015) 2083–2093. doi:10.1007/s13277-015-4003-0.
816 [41] C. Kilkenny, W.J. Browne, I.C. Cuthill, M. Emerson, D.G. Altman, Improving
817 bioscience research reporting: the ARRIVE guidelines for reporting animal
818 research, Osteoarthr. Cartil. 20 (2012) 256–260.
819 doi:10.1016/J.JOCA.2012.02.010.
820 [42] C.-C. Liang, A.Y. Park, J.-L. Guan, In vitro scratch assay: a convenient and
821 inexpensive method for analysis of cell migration in vitro, Nat. Protoc. 2 (2007)
822 329–333. doi:10.1038/nprot.2007.30.
823 [43] S. Cha, G. Johnson, Y.Z. Wadghiri, O. Jin, J. Babb, D. Zagzag, D.H. Turnbull,
824 Dynamic , Contrast-Enhanced Perfusion MRI in Mouse Gliomas : Correlation
825 With Histopathology, 855 (2003) 848–855. doi:10.1002/mrm.10446.
826 [44] G. Paxinos, K.B.J. Franklin, The mouse brain in stereotaxic coordinates: hard
827 cover edition., Acad. Press. 2nd Editio (2001) 360.
828 https://www.elsevier.com/books/paxinos-and-franklins-the-mouse-brain-in-
829 stereotaxic-coordinates-compact/franklin/978-0-12-816159-3 (accessed August
830 14, 2021).
831 [45] CCAC GUIDELINES, Can. Vet. J. 44 (2003) 631.
832 https://www.ncbi.nlm.nih.gov/pmc/articles/PMC340226/.
833 [46] I. Vermes, C. Haanen, H. Steffens-Nakken, C. Reutellingsperger, A novel assay
834 for apoptosis Flow cytometric detection of phosphatidylserine expression on
835 early apoptotic cells using fluorescein labelled Annexin V, J. Immunol. Methods.
836 184 (1995) 39–51. doi:https://doi.org/10.1016/0022-1759(95)00072-I.
837 [47] G. Barroso, S. Taylor, M. Morshedi, F. Manzur, F. Gaviño, S. Oehninger,
838 Mitochondrial membrane potential integrity and plasma membrane translocation
839 of phosphatidylserine as early apoptotic markers: a comparison of two different
840 sperm subpopulations, Fertil. Steril. 85 (2006) 149–154.
841 doi:https://doi.org/10.1016/j.fertnstert.2005.06.046.
842 [48] J. Skommer, D. Wlodkowic, W. Telford, J. Skommer, Z. Darzynkiewicz,
843 Apoptosis and beyond: cytometry in studies of programmed cell death, Methods
844 Cell Biol. 103 (2011) 55–98. doi:10.1016/B978-0-12-385493-3.00004-8.
845 [49] A. Wells, J. Grahovac, S. Wheeler, B. Ma, D. Lauffenburger, Targeting tumor

846 cell motility as a strategy against invasion and metastasis, Trends Pharmacol. Sci.
847 34 (2013) 283–289. doi:https://doi.org/10.1016/j.tips.2013.03.001.
848 [50] R.J. Eddy, M.D. Weidmann, V.P. Sharma, J.S. Condeelis, Tumor Cell
849 Invadopodia: Invasive Protrusions that Orchestrate Metastasis, Trends Cell Biol.
850 27 (2017) 595–607. doi:https://doi.org/10.1016/j.tcb.2017.03.003.
851 [51] J. Winkler, A. Abisoye-Ogunniyan, K.J. Metcalf, Z. Werb, Concepts of
852 extracellular matrix remodelling in tumour progression and metastasis, Nat.
853 Commun. 11 (2020) 5120. doi:10.1038/s41467-020-18794-x.
854 [52] J. Folkman, Angiogenesis in cancer, vascular, rheumatoid and other disease, Nat.
855 Med. 1 (1995) 27–30. doi:10.1038/nm0195-27.
856 [53] J. Folkman, Angiogenesis: an organizing principle for drug discovery?, 6 (2007)
857 273–286.
858 [54] T.C.G.A. TCGA, Comprehensive genomic characterization defines human
859 glioblastoma genes and core pathways, Nature. 455 (2008) 1061–1068.
860 doi:10.1038/nature07385.
861 [55] J. Langhans, L. Schneele, N. Trenkler, H. von Bandemer, L. Nonnenmacher, G.
862 Karpel-Massler, M.D. Siegelin, S. Zhou, M.-E. Halatsch, K.-M. Debatin, M.-A.
863 Westhoff, The effects of PI3K-mediated signalling on glioblastoma cell
864 behaviour, Oncogenesis. 6 (2017) 398. doi:10.1038/s41389-017-0004-8.
865 [56] D. Chen, D. Zuo, C. Luan, M. Liu, M. Na, L. Ran, Y. Sun, A. Persson, E.
866 Englund, L.G. Salford, E. Renström, X. Fan, E. Zhang, Glioma cell proliferation
867 controlled by ERK activity-dependent surface expression of PDGFRA, PLoS
868 One. 9 (2014). doi:10.1371/journal.pone.0087281.
869 [57] V. Frattini, V. Trifonov, J.M. Chan, A. Castano, M. Lia, F. Abate, S.T. Keir,
870 A.X. Ji, P. Zoppoli, F. Niola, C. Danussi, I. Dolgalev, P. Porrati, S. Pellegatta, A.
871 Heguy, G. Gupta, D.J. Pisapia, P. Canoll, J.N. Bruce, R.E. McLendon, H. Yan,
872 K. Aldape, G. Finocchiaro, T. Mikkelsen, G.G. Privé, D.D. Bigner, A. Lasorella,
873 R. Rabadan, A. Iavarone, The integrated landscape of driver genomic alterations
874 in glioblastoma, Nat. Genet. 45 (2013) 1141–1149. doi:10.1038/ng.2734.
875 [58] M. Miyai, H. Tomita, A. Soeda, H. Yano, T. Iwama, A. Hara, Current trends in
876 mouse models of glioblastoma, J. Neurooncol. 135 (2017) 423–432.
877 doi:10.1007/s11060-017-2626-2.

878 [59] E.W. Newcomb, D. Zagzag, CNS Cancer, CNS Cancer. (2009) 227–241.
879 doi:10.1007/978-1-60327-553-8.
880 [60] V.A. Kudryavtsev, A. V. Khokhlova, V.A. Mosina, E.I. Selivanova, A.E.
881 Kabakov, Induction of Hsp70 in tumor cells treated with inhibitors of the Hsp90
882 activity: A predictive marker and promising target for radiosensitization, PLoS
883 One. 12 (2017) 1–26. doi:10.1371/journal.pone.0173640.
884 [61] R. Bagatell, G.D. Paine-Murrieta, C.W. Taylor, E.J. Pulcini, S. Akinaga, I.J.
885 Benjamin, L. Whitesell, Induction of a heat shock factor 1-dependent stress
886 response alters the cytotoxic activity of Hsp90-binding agents, Clin. Cancer Res.
887 6 (2000) 3312–3318.
888 [62] L.R. Kelland, S.Y. Sharp, P.M. Rogers, T.G. Myers, P. Workman, DT-
889 Diaphorase expression and tumor cell sensitivity to 17-allylamino, 17-
890 demethoxygeldanamycin, an inhibitor of heat shock protein 90, J Natl Cancer
891 Inst. 91 (1999) 1940–1949. https://www.ncbi.nlm.nih.gov/pubmed/10564678.
892 [63] R.B. BADISA, S.F. DARLING-REED, P. JOSEPH, J.S. COOPERWOOD, L.M.
893 LATINWO, C.B. GOODMAN, Selective Cytotoxic Activities of Two Novel
894 Synthetic Drugs on Human Breast Carcinoma MCF-7 Cells, Anticancer Res. 29
895 (2009) 2993 LP – 2996. http://ar.iiarjournals.org/content/29/8/2993.abstract.
896 [64] W. Zhou, D.R. Wahl, Metabolic Abnormalities in Glioblastoma and Metabolic
897 Strategies to Overcome Treatment Resistance, Cancers (Basel). 11 (2019) 1231.
898 doi:10.3390/cancers11091231.
899 [65] M.G. Ormerod, F. Paul, M. Cheetham, X. -M Sun, Discrimination of apoptotic
900 thymocytes by forward light scatter, Cytometry. 21 (1995) 300–304.
901 doi:10.1002/cyto.990210311.
902 [66] S.M. Faisal, A. Comba, M.L. Varela, A.E. Argento, E. Brumley, C. Abel, M.G.
903 Castro, P.R. Lowenstein, The complex interactions between the cellular and non-
904 cellular components of the brain tumor microenvironmental landscape and their
905 therapeutic implications , Front. Oncol. . 12 (2022).
906 https://www.frontiersin.org/articles/10.3389/fonc.2022.1005069.
907 [67] F. Seker-Polat, N. Pinarbasi Degirmenci, I. Solaroglu, T. Bagci-Onder, Tumor
908 Cell Infiltration into the Brain in Glioblastoma: From Mechanisms to Clinical
909 Perspectives., Cancers (Basel). 14 (2022). doi:10.3390/cancers14020443.

910 [68] E.W. Newcomb, Y. Lukyanov, T. Schnee, M. Esencay, I. Fischer, D. Hong, Y.
911 Shao, D. Zagzag, The geldanamycin analogue 17-allylamino-17-
912 demethoxygeldanamycin inhibits the growth of GL261 glioma cells in vitro and
913 in vivo, Anticancer. Drugs. 18 (2007) 875–882.
914 doi:10.1097/CAD.0b013e3281430df8.
915 [69] B.K. Eustace, T. Sakurai, J.K. Stewart, D. Yimlamai, C. Unger, C. Zehetmeier,
916 B. Lain, C. Torella, S.W. Henning, G. Beste, B.T. Scroggins, L. Neckers, L.L.
917 Ilag, D.G. Jay, Functional proteomic screens reveal an essential extracellular role
918 for hsp90 alpha in cancer cell invasiveness, Nat Cell Biol. 6 (2004) 507–514.
919 doi:10.1038/ncb1131.
920 [70] E.C. Brantley, E.N. Benveniste, Signal Transducer and Activator of
921 Transcription-3: A Molecular Hub for Signaling Pathways in Gliomas, Mol.
922 Cancer Res. 6 (2008) 675. doi:10.1158/1541-7786.MCR-07-2180.
923 [71] F. Azuaje, K. Tiemann, S.P. Niclou, Therapeutic control and resistance of the
924 EGFR-driven signaling network in glioblastoma, Cell Commun. Signal. 13
925 (2015) 23. doi:10.1186/s12964-015-0098-6.
926 [72] G.L. Johnson, R. Lapadat, Mitogen-Activated Protein Kinase Pathways Mediated
927 by ERK, JNK, and p38 Protein Kinases, Science (80-.). 298 (2002) 1911.
928 doi:10.1126/science.1072682.
929 [73] D.I. Duron, W. Lei, N.K. Barker, C. Stine, S. Mishra, B.S.J. Blagg, P.R.
930 Langlais, J.M. Streicher, Inhibition of Hsp90 in the spinal cord enhances the
931 antinociceptive effects of morphine by activating an ERK-RSK pathway., Sci.
932 Signal. 13 (2020). doi:10.1126/scisignal.aaz1854.
933 [74] J.M. Streicher, The Role of Heat Shock Proteins in Regulating Receptor Signal
934 Transduction, Mol. Pharmacol. 95 (2019) 468 LP – 474.
935 doi:10.1124/mol.118.114652.
936 [75] G. Niu, K.L. Wright, M. Huang, L. Song, E. Haura, J. Turkson, S. Zhang, T.
937 Wang, D. Sinibaldi, D. Coppola, R. Heller, L.M. Ellis, J. Karras, J. Bromberg, D.
938 Pardoll, R. Jove, Constitutive Stat3 activity up-regulates VEGF expression and
939 tumor angiogenesis, (2008) 2000–2008. doi:10.1038/sj/onc/1205260.
940 [76] Q. Xu, J. Briggs, S. Park, G. Niu, M. Kortylewski, S. Zhang, T. Gritsko, J.
941 Turkson, H. Kay, G.L. Semenza, J.Q. Cheng, R. Jove, H. Yu, Targeting Stat3

942 blocks both HIF-1 and VEGF expression induced by multiple oncogenic growth
943 signaling pathways, Oncogene. (2005). doi:10.1038/sj.onc.1208719.
944 [77] K. Palmowski, O. Winz, A. Rix, J. Bzyl, F.F. Behrendt, F.A. Verburg, F.M.
945 Mottaghy, M. Palmowski, Accuracy of a clinical PET/CT vs. a preclinical μPET
946 system for monitoring treatment effects in tumour xenografts., Eur. J. Radiol. 82
947 (2013) 1318–1324. doi:10.1016/j.ejrad.2013.01.028.
948 [78] S. Kirschner, B. Mürle, M. Felix, A. Arns, C. Groden, F. Wenz, A. Hug, G.
949 Glatting, M. Kramer, F.A. Giordano, M.A. Brockmann, Imaging of Orthotopic
950 Glioblastoma Xenografts in Mice Using a Clinical CT Scanner: Comparison with
951 Micro-CT and Histology, PLoS One. 11 (2016) e0165994.
952 doi:10.1371/journal.pone.0165994.
953 [79] M.A. Hofman, Size and Shape of the Cerebral Cortex in Mammals, Brain.
954 Behav. Evol. 32 (1988) 17–26. doi:10.1159/000116529.
955 [80] M. Hofman, Evolution of the human brain: when bigger is better , Front.
956 Neuroanat. . 8 (2014) 15.
957 https://www.frontiersin.org/article/10.3389/fnana.2014.00015.
958 [81] A. Welch, M. Mingarelli, G. Riedel, B. Platt, Mapping changes in mouse brain
959 metabolism with PET/CT., J. Nucl. Med. 54 (2013) 1946–1953.
960 doi:10.2967/jnumed.113.121509.
961 [82] N. Ferrara, Pathways mediating VEGF-independent tumor angiogenesis,
962 Cytokine Growth Factor Rev. 21 (2010) 21–26.
963 doi:https://doi.org/10.1016/j.cytogfr.2009.11.003.
964